ULTRASONIC IMAGING 15, 134-149 (1993)

PRODUCING DEEP DEPTH OF FIELD AND DEPTH-INDEPENDENT RESOLUTION IN NDE WITH LIMITED DIFFRACTION BEAMS

Jian-yu Lu and James F. Greenleaf

Biodynamics Research Unit
Department of Physiology and Biophysics
Mayo Clinic and Foundation
Rochester, MN 55905

Limited diffraction beams, such as Durnin's J_0 Bessel beam, are a class of nonspreading solutions to the isotropic/homogeneous scalar wave equation. These beams can be approximately produced with finite aperture and energy over a deep depth of field. In this paper, we report the application of a broadband J_0 Bessel beam to nondestructive evaluation (NDE) of materials. Pulse-echo images of a stainless steel block phantom were obtained with both the J_0 Bessel beam and a conventional focused Gaussian beam. Results show that uniformly high resolutions were obtained with the J_0 Bessel beam over a large distance. In addition, the lateral resolution of the J_0 Bessel beam is almost independent of the speed of sound of the materials inspected. In contrast, the lateral resolution of images obtained with the conventional focused Gaussian beam changes dramatically with the distance and the focal length of the beam in water is greatly reduced by the steel block. Therefore, limited diffraction beams could be useful for nondestructive evaluation of materials of different speeds of sound. Restoration of pulse-echo images obtained with these beams could be simplified.

Key words: Bessel beams; imaging; image restoration; limited diffraction beams; materials; nondestructive evaluation; wave equations; X waves.

I. INTRODUCTION

There are two types of solutions to the isotropic/homogeneous scalar wave equation that govern the propagation of acoustic waves in isotropic/homogeneous media and electromagnetic waves in free space that are of interest in imaging. One represents conventional diffracting waves such as beams produced from Gaussian weighted apertures and focused beams. The other represents waves that can propagate to infinite distance without spreading, such as Durnin's Bessel beams, and were termed by Durnin as "nondiffracting" or "diffraction-free" beams [1]. (Because Durnin's terminologies are controversial, in the following, we will use a new terminology "limited diffraction beams"). Exact limited diffraction beams can only exist

0161-7346/93 $5.00

theoretically because they require an infinite aperture and energy. However, these beams can be closely approximated over a large propagation distance with a sufficiently large aperture and amount of energy. This character of the limited diffraction beams is distinct from the conventional diffracting beams that remain diffracting no matter how big the aperture and how large the amount of energy that is used to produce them.

The first localized solution to the isotropic/homogeneous scalar wave equation was reported by Brittingham in 1983 in electromagnetics [2]. Brittingham termed his new solution "focus wave mode". Two years later, in 1985, Ziolkowski discovered a new focus wave mode and found a way to construct new localized solutions by Laplace transform [3]. Further, in 1989, Ziolkowski et al. constructed localized waves of a finite total energy that he called "modified power spectrum pulses" and produced them experimentally with acoustic superposition [4]. Independent of Brittingham and Ziolkowski et al., Durnin discovered the first limited diffraction beam in optics in 1987 [1] and constructed a J_0 Bessel beam with an optical experiment [5]. Following Durnin's work, Hsu et al. have produced a narrow band J_0 Bessel beam with an acoustic transducer using a nonuniform poling technique [6]. We have closely approximated a J_0 Bessel beam with a broadband ultrasonic annular array transducer of a finite aperture and suggested its applications to medical imaging and tissue characterization [7–18]. Campbell and Soloway had a similar idea to produce a J_0 Bessel beam with an acoustic annular array transducer [19]. In addition, we have discovered recently families of generalized limited diffraction beam solutions to the isotropic/homogeneous scalar wave equation. These solutions include some of the limited diffraction beams known previously, such as the Bessel beams, in addition to an infinity of new beams. One family of the new solutions represents waves that have an X-like shape in a plane along the wave axis and were termed "X waves" [20–22]. The theoretical X waves are nonspreading in both lateral and axial directions (nondispersive) as they propagate to an infinite distance. Since the X waves are nonspreading and nondispersive, pulse-echo images with these waves could be restored to produce high resolution images if the materials to be imaged do not present severe phase aberration and strong multiple scattering [23].

In nondestructive evaluation of materials, methods used in medical imaging for improving the lateral resolution and increasing the depth of field of the conventional beams, such as multiple transmits focused at different depths and dynamically focused receive [24], are difficult to apply because of the diversity of the speed of sound of the materials inspected. Since the limited diffraction beams focus over a large depth of field, they could be useful to obtain high resolution images over large depth of interest. In this paper, we study experimentally the application of the limited diffraction beam, specifically, a broadband J_0 Bessel beam (we have extended Durnin's Bessel beam from monochromatic to broadband for a pulse-echo imaging application [8]) to nondestructive evaluation (NDE) of materials. The J_0 Bessel beam was produced by a 10-element, 2.5 MHz central frequency, and 50 mm diameter broadband annular array transducer. Pulse-echo images of a stainless steel block phantom that contains 11 parallel holes of different sizes were obtained with both the J_0 Bessel beam and a conventional focused Gaussian beam (the focal length was about 120 mm in water). The phantom was placed in water at several distances away from the surface of the transducer. Results show that approximately uniform -6-dB widths (their averages are about 2.44 and 2.63 mm, respectively) of the lateral and axial line plots of the images of a 1 mm diameter hole were obtained with the J_0 Bessel beam over a large distance (about 230 mm). This means that the point spread function of the J_0 Bessel beam imaging system

is approximately depth-independent (shift-invariant). In addition, the lateral resolution of the J_0 Bessel beam is almost independent of the speed of sound of the materials inspected within the depth of field of the beam (the steel has a much higher speed of sound than water). In contrast, the -6-dB width of the lateral line plot of the images of the 1 mm diameter hole obtained with the conventional focused Gaussian beam changes dramatically (from about 3 mm to over 7 mm) in the distance (230 mm) and the focal length of the Gaussian beam in water is greatly reduced by the steel block (good images are obtained only near the focal length). This demonstrates that the limited diffraction beams could be useful for nondestructive evaluation of materials of different speeds of sound because their lateral resolution is almost independent of the speed of sound of materials inspected within the depth of field (of course, higher speed of sound will reduce the depth of field). In addition, the restoration of pulse-echo images could be simplified because the point spread function of the imaging system is approximately depth-independent [10,23].

In the next section, a theoretical preliminary of the limited diffraction beams is presented. In section III, the imaging experiment on a steel block using an ultrasonic J_0 Bessel beam and a conventional focused Gaussian beam is described. The experiment results are reported in section IV, and in sections V and VI, we give a brief discussion and a conclusion.

II. THEORY

An n-dimensional isotropic/homogeneous scalar wave equation is given by [25]

$$\left[\sum_{j=1}^{n}\frac{\partial^2}{\partial x_j^2}-\frac{1}{c^2}\frac{\partial^2}{\partial t^2}\right]\Phi=0, \tag{1}$$

where x_j, $(j=1,2,\cdots,n)$, are n rectangular spatial coordinates, n is an integer, t is time, c is a constant (represents the speed of sound of a medium), and $\Phi=\Phi(x_1,x_2,\cdots,x_n;t)$ represents an n-dimensional wave field.

A special solution of the wave equation is given by [10]:

$$\Phi(x_1,x_2,\cdots,x_n;t)=f(s), \tag{2}$$

where

$$s=\sum_{j=1}^{n-1}D_jx_j+D_n(x_n-c_1t),\quad(n\geq 1), \tag{3}$$

$$c_1=\pm c\sqrt{1+\sum_{j=1}^{n-1}D_j^2/D_n^2},\quad(n\geq 1), \tag{4}$$

and where D_j are any complex coefficients and are independent of the spatial and time variables, $f(s)$ is any well-behaved complex function of s, and $n \neq 0$ (if $n = 0$, $f(s)$ is only a function of time and does not represent a wave). In the following, the "+" sign in Eq. (4) is chosen to represent waves going in positive direction of axis D_n.

Durnin's Bessel beams [1] can be derived from Eq. (2) by choosing the forms of the coefficients and integrating over some of the free parameters [10,20]. Letting $n = 3, x_1 = x,\ x_2 = y,\ x_3 = z,\ f(s) = e^s,\ D_1 = -i\alpha\cos\theta,\ D_2 = i\alpha\sin\theta$, and $D_3 = i\beta$, where α and θ are free parameters which are independent of the spatial variables, $\vec{r} = (x, y, z)$, and time, t, $\beta = \sqrt{(\omega/c)^2 - \alpha^2} = \omega/c_1$ (where $\omega/c \geq \alpha$), and ω is angular frequency, and averaging $f(s)$ by integration with respect to θ from $-\pi$ to π, one obtains the zeroth order Bessel beam [1]:

$$\Phi_{J_0} = J_0(\alpha r)e^{i(\beta z - \omega t)}, \tag{5}$$

where $r = \sqrt{x^2 + y^2}$ is a radial distance from the axis of the beam.

In the next section, we will describe pulse-echo imaging experiments using a broadband J_0 Bessel beam and a conventional focused Gaussian beam.

III. EXPERIMENTAL SYSTEM

A. TRANSDUCER

A 10–element, 2.5 MHz central frequency, and 50 mm diameter broadband ultrasonic annular array transducer (Fig. 1) was used to produce either the J_0 Bessel beam or a conventional focused Gaussian beam. The transducer elements are formed by cutting the back electrode into 10 rings and the width of each ring corresponds to the width of one lobe of the function, $J_0(\alpha r)$, where α = 1202.45 m^{-1} [7,8]. The −6-dB pulse-echo bandwidth of the transducer is about 50% of its central frequency. A stepwise approximated Bessel beam was produced by applying voltages which correspond to the maxima and phases of the lobes of the function, $J_0(\alpha r)$. Its −6-dB main beam width is about 2.54 mm [7]. For the focused Gaussian beam, a stepwise approximated Gaussian aperture weighting function that has a FWHM (full width at half maximum) of 25 mm was applied to the annular array, and a plexiglass lens was attached to the front surface of the transducer to focus the beam in water at a depth of about 120 mm. In receive, the aperture weightings were the same as those in the transmit. Pulse-echo envelope images were studied.

B. PHANTOM DESCRIPTION

We have made a stainless steel (type 303) block phantom with a design shown in figure 2 (a photograph of the phantom is shown in figure 3). The size of the phantom is 100 mm (width) x 50 mm (height) x 50 mm (thickness). Eleven parallel holes were drilled from front to back through the phantom of thickness of 50 mm. There are 4 groups of holes with diameters of 10 mm (1 hole), 5 mm (1 hole), 2.5 mm (1 hole), and 1 mm (8 holes),

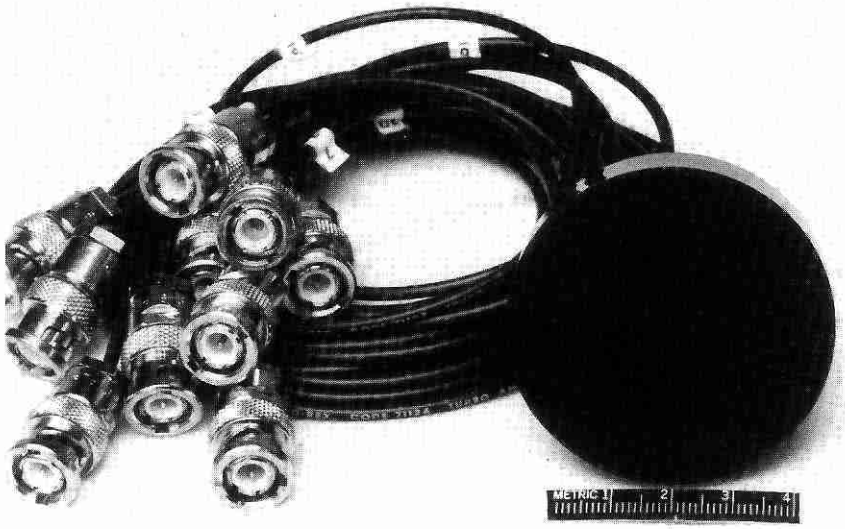

Fig. 1 Photograph of the 10-element, 2.5 MHz central frequency, and 50 mm diameter broadband annular array transducer used in the experiment.

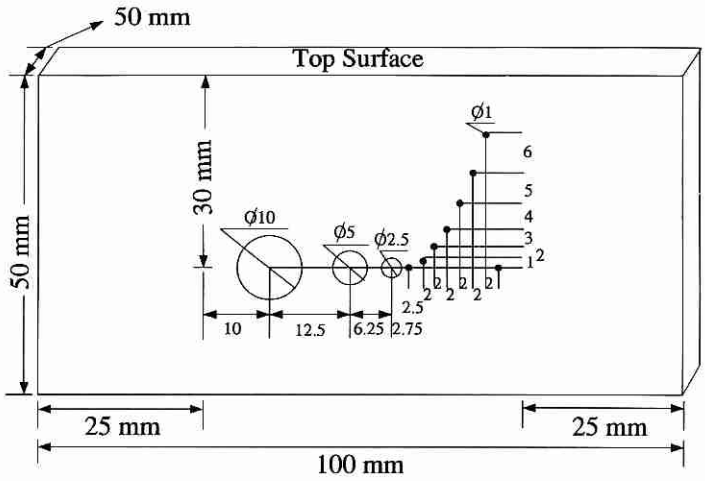

Fig. 2 Geometry of a phantom made from a stainless steel (Type 303). The phantom has 11 holes driven through the steel block from the front to the back. These holes have 4 different diameters: 10 mm (1 hole), 5 mm (1 hole), 2.5 mm (1 hole), and 1 mm (8 holes). They act as "flaws" and form a resolution pattern located at about the center of the phantom. The dimension of the phantom is 100 mm (width) x 50 mm (height) x 50 mm (thickness).

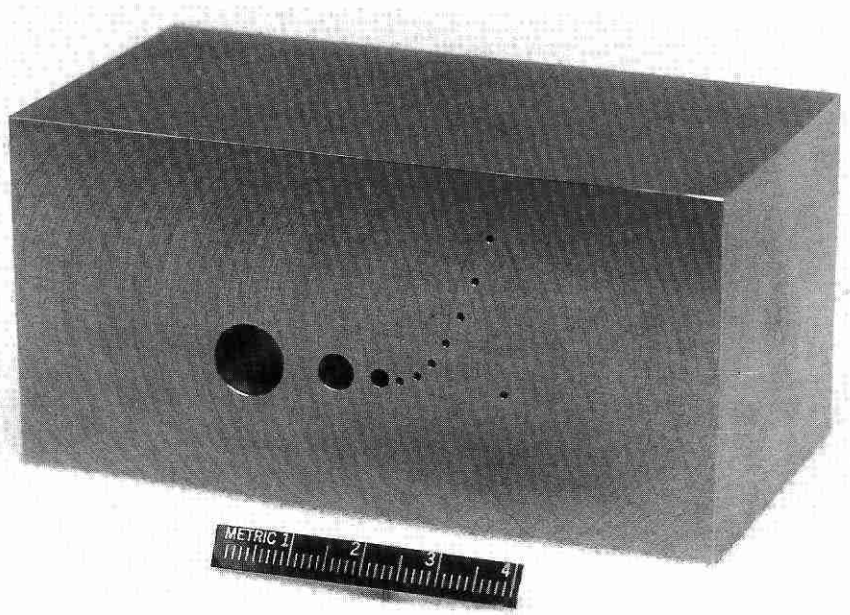

Fig. 3 Photograph of the stainless steel phantom described in figure 2.

respectively. The relative positions of the holes in the steel block are described in figure 2. These holes were used as models of "flaws" in the material.

C. EXPERIMENT SETUP

Figure 4 shows a block diagram of the experimental setup. Both the transducer and the phantom were immersed in a water tank. A Polynomial Waveform Synthesizer (Model Data 2045) produced a broadband pulse (of about one and one half cycle time duration at a central frequency of 2.5 MHz). The pulse was amplified and weighted to produce either the J_0 Bessel beam or the focused Gaussian beam using a transmitting/receiving electronic box made in our lab. The 10 elements of the transducer were driven simultaneously, and the echoes returned from the phantom were weighted and summed to produce either the J_0 Bessel or the focused Gaussian responses. The summed signal was amplified linearly and digitized at a sampling rate of 20 megasamples/second. These data were transferred to a SUN workstation for calculating analytic signals (envelopes) from the rf echoes and pulse-echo images were displayed.

The data acquisition system was controlled by a minicomputer (MC68000). When the transducer was moved to a desired position with a stepping motor, the Polynomial Waveform Synthesizer was triggered to generate an electrical pulse to excite the transducer. After a preset delay time, the A/D converter digitized the echo signals and stored them in the

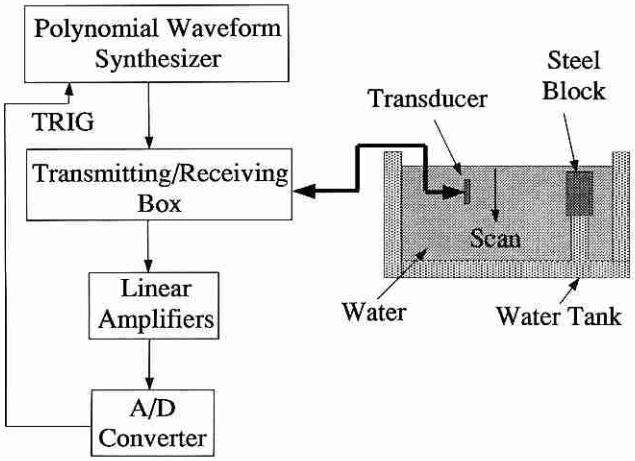

Fig. 4 Block diagram of experiment. The transducer shown in figure 1 was put in a water tank and scanned over the top surface of the phantom (Fig. 2) and echoes are recorded to form pulse-echo images.

memory of the minicomputer. The above processes were repeated until all the A-lines from the phantom were acquired. The center of the transducer was scanned across the middle of the holes in the stainless steel block phantom.

To compare the depth of field of the J_0 Bessel beam and the focused Gaussian beam in the nondestructive evaluation of materials, we made scans at several distances, Z, which are the distances between the transducer surface and the center of the rightmost 1 mm diameter hole (Fig. 2). The normalized distances, Z/D, are also used, where D = 50 mm is the diameter of the transducer.

IV. RESULTS

The pulse-echo images (envelopes) of the stainless steel block phantom obtained with the J_0 Bessel beam and the focused Gaussian beam are shown in figures 5 and 6, respectively. For the Bessel beam, the smallest Z/D is 0.6 at which the top surface of the steel block almost touches the front surface of the transducer. However, for the focused Gaussian beam, the smallest Z/D is 1.1 because a plexiglass lens was attached to the front surface of the transducer. Figures 7 and 8 are lateral (full lines) and axial (dotted lines) line plots of the images of the rightmost 1 mm diameter hole at different Z/D corresponding to figures 5 and 6, respectively. The last panel in figure 7 or 8 shows the dependence of the -6-dB width of the lateral and axial line plots of the hole images over Z/D. The results show that the images obtained with the J_0 Bessel beam are of approximately uniform high lateral and axial resolutions over a deep depth of field (about 216 mm in water [7]). Most of the "flaws" are

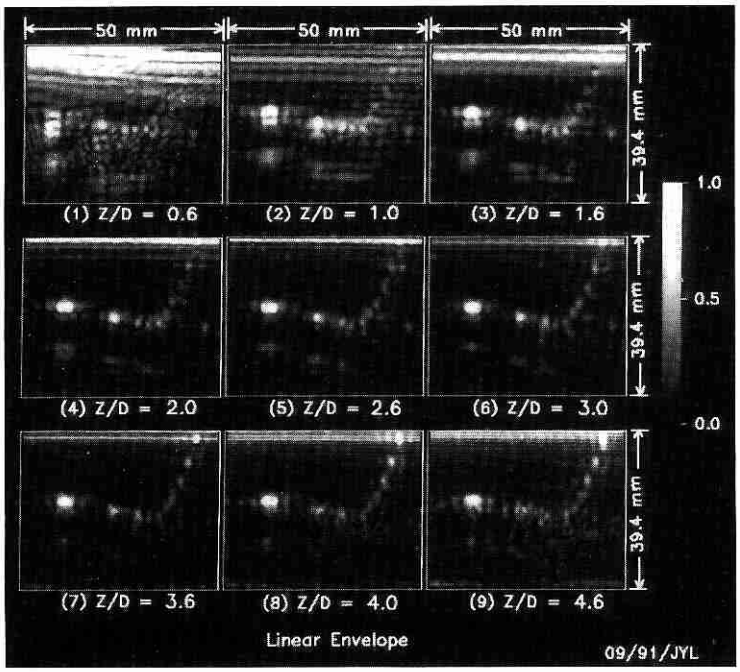

Fig. 5 Envelopes of experimentally measured pulse-echo images of a cross section of the stainless steel block phantom in figure 2 obtained by a J_0 Bessel beam. Panels (1) to (9) correspond to images obtained at Z/D = 0.6, 1.0, 1.6, 2.0, 2.6, 3.0, 3.6, 4.0, and 4.6, respectively (where Z is the axial distance between the surface of the transducer and the center of the rightmost 1 mm hole in figure 2, and D = 50 mm is the diameter of the transducer). Panel size is 50 mm (width) $\times$ 39.4 mm (height) which represents a window that avoids most of the strong multiple reflections between the flat surfaces of the transducer and the phantom, and strong ringing from the water-phantom interface. The gray levels are normalized to the maximum of the hole images of each panel.

clearly resolved, especially in the midrange of the Z/D. With the focused Gaussian beam, the images obtained have high lateral resolution only near the focal depth of the beam. Since the steel block has a higher speed of sound than water, the incident focused Gaussian beam is refocused by the steel block due to the refraction (in this case, the focal length is shortened from the original 120 mm focal length). Apparently, the refocusing phenomenon becomes stronger as the difference of the speed of sound between the coupling media and the testing objects increases and diminishes if the difference decreases. The line focusing properties of the limited diffraction beams will not be changed by the materials inspected within their deep depth of field (of course, high speed of sound reduces the depth of field). This could simplify procedures for inspecting materials of different speeds of sound while keeping a high lateral resolution.

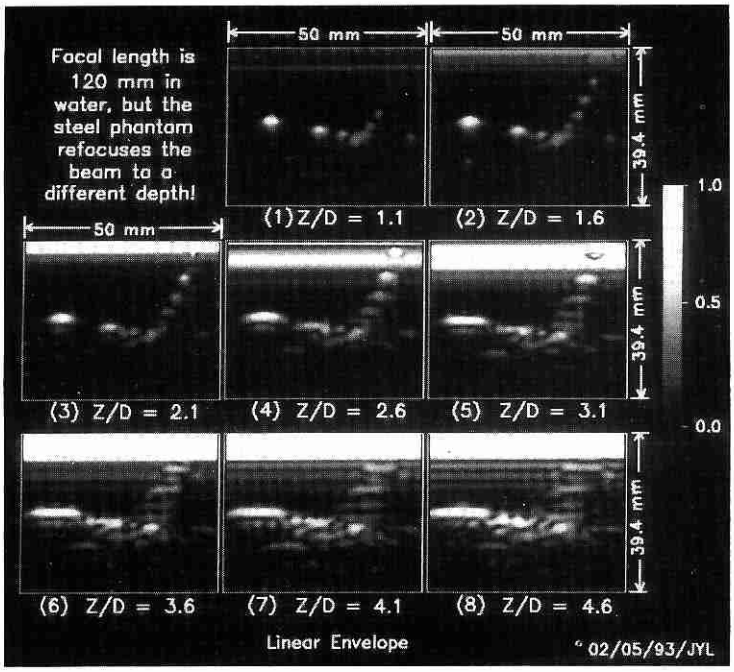

Fig. 6 Pulse-echo image obtained with a conventional focused Gaussian beam (focal length is about 120 mm in water and the full width at half maximum of the beam at the transducer surface is 25 mm). It has the same format as that of figure 5, but the first panel starts from Z/D = 1.1 in order to allow a plexiglass lens inserted between the surface of the transducer and the top surface of the steel block phantom. The eight panels correspond to Z/D of 1.1, 1.6, 2.1, 2.6, 3.1, 3.6, 4.1, and 4.6, respectively. High speed of sound of the steel block phantom shortened the focal length of the transducer.

V. DISCUSSION

A. RESOLUTION AND DEPTH OF FIELD

Images obtained with the J_0 Bessel beam have approximately uniform high lateral and axial resolutions over a deep depth of field (the depth of field of the Bessel beam is about 216 mm in water with the transducer parameters given in III). The average -6-dB lateral and axial widths of the line plots of the images of the rightmost 1 mm diameter hole (Fig. 2) are about 2.44 mm and 2.63 mm, respectively. Almost all the "flaws" of the stainless steel block phantom are resolved in all the depths (Fig. 5). The depth of field of the J_0 Bessel beam could be further increased by raising the central frequency [1]. In the images produced with the conventional focused Gaussian beam, the -6-dB lateral width of the line plots of

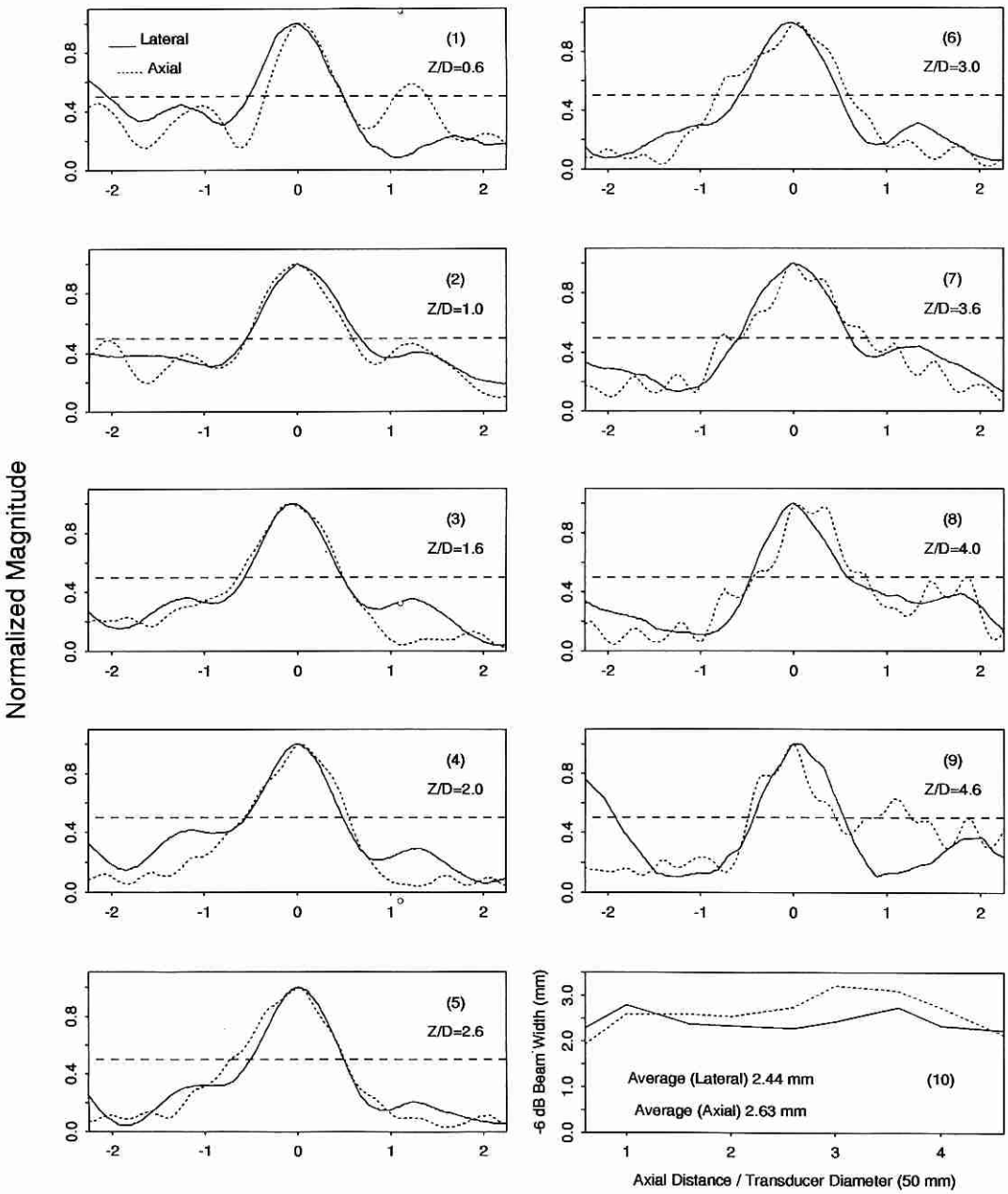

Fig. 7 Lateral (full lines) and axial (dotted lines) line plots of the images of the rightmost 1 mm diameter hole (30 mm down from the top surface of the phantom) obtained with the J_0 Bessel beam at different Z/D values corresponding to those in figure 5 (see Panels (1) to (9)). Panel (10) shows the -6-dB width of the lateral and axial line plots of the images versus Z/D. The central wavelength in steel is about 2.28 mm and transducer diameter is 50 mm.

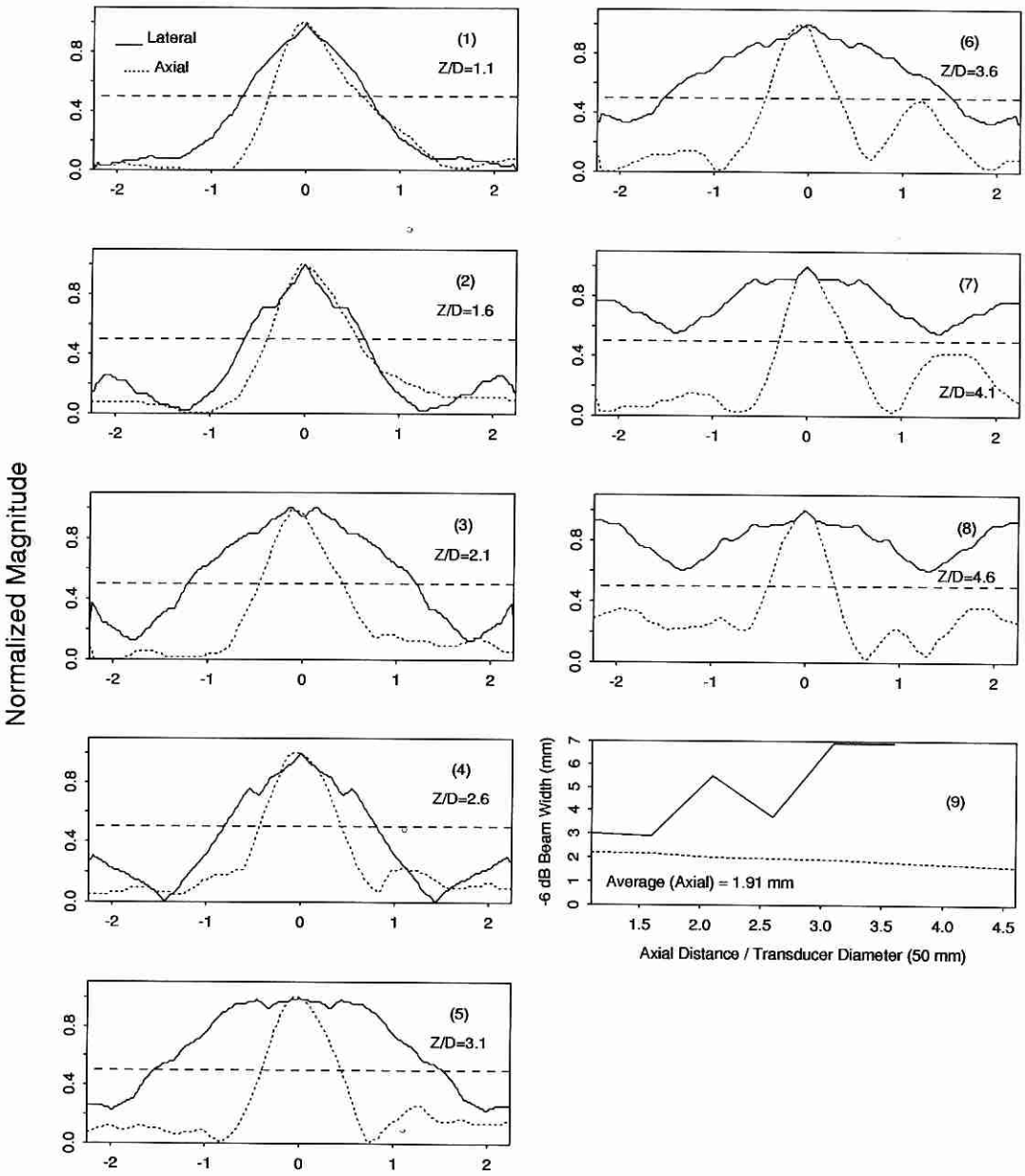

Fig. 8 Lateral (full lines) and axial (dotted lines) line plots of images of the rightmost 1 mm diameter hole obtained with the conventional focused Gaussian beam corresponding to those in figure 6. It has a similar format as that of figure 7. The parameters of the beam are given in the caption of figure 6. For the lateral line plots, the right side of the peaks are symmetrically added from the data of the left since the data on the right are not available (out of boundaries of the images in figure 6).

the images of the rightmost 1 mm hole changes dramatically with the depth (increased from about 3 mm to over 7 mm) although the axial width of the images stays about the same (1.91 mm). The quality of the images at the depths that are out of focus is so poor that the interpretation of the structure of the steel block is difficult (Fig. 6).

The axial resolution of the images in figures 5 and 6 depends only upon the central frequency and bandwidth of the transducer. Unlike medical imaging (where ultrasound is mainly used to examine biological soft tissues that have a relatively low speed of sound around 1.5 mm/μs), materials in nondestructive evaluation could have a high speed of sound and hence have a long wavelength at a given central frequency (for example, the speed of sound of the 303 stainless steel is about 5.7 mm/μs). To obtain images of axial resolution similar to that of medical imaging, transducers of much higher central frequency and broader bandwidth are needed. The bandwidth of a transducer can be maximized by matching the acoustical impedance of the transducer to both its front and backing materials as well as the materials to be inspected. Matching between the driving circuits and the electrical impedance of the transducer will also help to increase the bandwidth.

Both the lateral and axial resolutions could also be increased by a deconvolution (image restoration) method [10, 26–27] if the materials imaged do not present significant phase aberration and strong multiple scattering. Imaging systems using conventional beams have depth-dependent point spread functions (shift-variant imaging systems) and thus their image restoration would be complex. The images must be subdivided into many pieces so that each has a point spread function that is approximately depth-independent and is restored separately. In contrast, imaging systems using limited diffraction beams will have much less variation in their point spread functions. For example, the Bessel beams (pulses) vary only slightly their pulse durations (dispersion) with depth but not their lateral beamwidths in the depth of field [19]. X waves will not change both their pulse durations and lateral beamwidths with depth in the depth of field [20–22]. Therefore, limited diffracting beams potentially offer advantages for deconvolution and restoration approaches [10,23].

B. INFLUENCE OF SPEED OF SOUND

From Eq. (5), it is seen that the speed of sound of materials inspected do not affect the main lobe width of the J_0 Bessel beam if $\omega/c > \alpha$ (the condition that the Bessel beam exists) [19]. Therefore, the lateral resolution of images with the J_0 Bessel beam will stay about constant within its depth of field (Fig. 5). This means that the same J_0 Bessel beam can be used to evaluate materials of different speeds of sound at the same high lateral resolution. Other limited diffraction beams such as the X waves will have approximately the same lateral beamwidth in materials of different speeds of sound. (At a higher speed of sound, the Axicon angle of the X wave will be increased which will shorten the depth of field, while its main beam width stays approximately unchanged because the central wavelength is increased [20]. At a lower speed of sound, the situation is reversed). The conventional focused Gaussian beam, as can be seen from figure 6, produces a focal length depending on the speed of sound of the materials inspected (the focal length of the transducer is short at a high speed of sound and long at a low speed of sound). To achieve the best results, either the focal length of the transducer or the distance between the region of interest and the transducer needs to be

adjusted for materials of different speeds of sound. This is inconvenient and can be avoided by using a J_0 Bessel beam or other limited diffraction beams such as a band-limited X wave.

Although it is argued that a dynamically focused annular array could be used to obtain images of large depth of field and lower sidelobes, it is inconvenient to apply such an array to imaging of materials of different speeds of sound since the focal length decreases as the speed of sound of the materials imaged increases (the transmit pulse will travel ahead of receiving focus if the speed of sound increases) or *vice versa*. This requires that the electronic system of the array must be adjusted constantly to match the speed of sound of the materials inspected. In addition, images obtained with dynamically focused arrays will still have a depth-dependent lateral resolution since the f-number of the array changes with depth and their restoration process would be complex.

C. FLAW CHARACTERIZATION

For the "flaws" of similar shapes (all are cylinders in figure 2), images of bigger "flaws" appear brighter and larger with the J_0 Bessel beam (Fig. 5). This is because the bigger "flaws" reflect more ultrasound energy in a wider lateral extent. This feature can be used as a flaw characterization. In figure 6, however, where the conventional focused Gaussian beam is used, the sizes and brightness of the images of the "flaws" depend not only on the sizes of the "flaws", but the strength and width of the incident beams. The missing lower part of the big holes in both figures 5 and 6 is caused by shadows of the upper part of the holes which blocks the ultrasound energy.

D. ARTIFACTS

There are two types of artifacts shown in the results. One is caused by multiple reflections between the surfaces of transducer and the steel block and reverberation inside the steel block. From figures 5 and 6, it is seen that the multiple reflections have strong impact when Z/D values are small. The strong multiple reflections could be dramatically reduced if we couple the transducer to the polished material surface with a special fluid suitable for nondestructive evaluation of metals, instead of water, and use a transducer whose impedance is close to that of the steel to provide better impedance matching (the transducer used in the experiment was originally designed for medical ultrasound and, therefore, has a lower impedance compared to that of the steel). Contact scans of a lubricated polished material surface will increase the detectability of flaws close to the top surface of the steel block (some of "flaws" of the steel block are washed away in both figures 5 and 6 by the strong ringing of the incident pulse caused by the impedance mismatch of the water-steel interface). The other artifacts (secondary images shown beneath the main objects in both figures 5 and 6) might come from shear waves induced by the surfaces of the holes that have an angle with the incident waves. This kind of artifact would be difficult to eliminate.

E. ELECTRONIC NOISE

Electronic noise will deteriorate the image quality if the received echo signals are too weak. Electronic noise is seen in figures 5 and 6 at larger Z/D values. The echo signals are weak in our experiment because the water-steel interface reflects most of the ultrasound

energy, and only a small portion of energy transmits through into the stainless steel block to carry back information regarding its structure. The detection sensitivity of the flaws will be increased if a contact scan with a transducer of a better impedance matching is used.

F. SIDELOBES AND SIGNAL-TO-NOISE RATIO

The sidelobes of a J_0 Bessel beam are larger than those of conventional focused beams at their foci. Artifacts caused by sidelobes can be seen at the sides of each "flaw" image. The sidelobes are also a source of multiple scattering when the materials inspected have a lot of randomly distributed flaws, which reduces the signal-to-noise ratio. Fortunately, in most nondestructive evaluation applications, ultrasound energy is used to examine individual flaws like cracks, cavities, and quality of welding joints. In these examinations, high resolution is more important than high contrast for evaluating material quality. For the conventional focused Gaussian beam, low sidelobe images are obtained only near its focal length. Away from the focus, the signal-to-noise ratio degrades severely.

VI. CONCLUSION

One of the limited diffraction beams, specifically the J_0 Bessel beam, was used for the nondestructive evaluation of a stainless steel (type 303) block. Pulse-echo images were obtained. The results demonstrate that images obtained with the J_0 Bessel beam have an approximately uniform high resolution over a deep depth of field of the beam. Images obtained with a conventional focused Gaussian beam have only high resolution near its focal length and the focal length of the beam changes with the speed of sound of the materials inspected. With the J_0 Bessel beam, the lateral resolution of pulse-echo images will not change with speed of sound of materials inspected within the depth of field of the beam. Other limited diffraction beams would have similar properties. Thus, limited diffraction beams should simplify the nondestructive evaluation of materials of different speeds of sound. In addition, the point spread function of the pulse-echo imaging system of a finite aperture limited diffraction beam will be approximately depth-independent (shift-invariant) over a large distance. Restoration of the images obtained by such system would be much simpler as compared to restoration of those obtained by a shift-variant system such as the conventional focused Gaussian beam. Therefore, the limited diffraction beams could be very useful for nondestructive evaluation of materials in addition to medical imaging and tissue characterization [7–18,20–22].

ACKNOWLEDGMENTS

The authors would like to thank Randall R. Kinnick for making the transmitting/receiving electronic box for the experiment. Discussions with Drs. E. P. Papadakis and Timothy Gray of Iowa State University are appreciated. The authors appreciate the secretarial assistance of Elaine C. Quarve and the graphic assistance of Christine A. Welch. This work was supported in part by grants CA 43920 and CA 54212 from the National Institutes of Health.

REFERENCES

[1] Durnin, J., Exact solutions for nondiffracting beams. I. The scalar theory, *J. Opt. Soc. Am. 4*, 651–654 (1987).

[2] Brittingham, J. B., Focus wave modes in homogeneous Maxwell's equations: transverse electric mode, *J. Appl. Phys. 54*, 1179–1189 (1983).

[3] Ziolkowski, R. W., Exact solutions of the wave equation with complex source locations, *J. Math. Phys. 26*, 861–863 (1985).

[4] Ziolkowski, R. W., Lewis, D. K., and Cook, B. D., Evidence of localized wave transmission, *Phys. Rev. Lett. 62*, 147–150 (1989).

[5] Durnin, J., Miceli, J. J., Jr., and Eberly, J. H., Diffraction-free beams, *Phys. Rev. Lett. 58*, 1499–1501 (1987).

[6] Hsu, D. K., Margetan, F. J., and Thompson, D. O., Bessel beam ultrasonic transducer: fabrication method and experimental results, *Appl. Phys. Lett. 55*, 2066–2068 (1989).

[7] Lu, J-y., and Greenleaf, J. F., Ultrasonic nondiffracting transducer for medical imaging, *IEEE Trans. Ultrason. Ferro. Freq. Control 37*, 438–447 (1990).

[8] Lu, J-y., and Greenleaf, J. F., Pulse-echo imaging using a nondiffracting beam transducer, *Ultrasound Med. Biol. 17*, 265–281 (1991).

[9] Lu, J-y., and Greenleaf, J. F., Evaluation of a Nondiffracting Transducer for Tissue Characterization, in *IEEE 1990 Ultrason. Symp. Proc.*, vol. 2, pp. 795–798 (IEEE Cat. No. 90CH2938-9).

[10] Lu, J-y., and Greenleaf, J. F., Diffraction-limited Beams and Their Applications for Ultrasonic Imaging and Tissue Characterization, in *New Developments in Ultrasonic Transducers and Transducer Systems*, F. L. Lizzi, ed., Proc. SPIE, vol. 1733, pp. 92–119 (1992).

[11] Lu, J-y., and Greenleaf, J. F., Formation and propagation of limited diffraction beams, in *Acoustic Imaging 20*, Ben-li Gu, ed. (to be published).

[12] Lu, J-y., and Greenleaf, J. F., Steering of Limited Diffraction Beams with a Two-dimensional Array Transducer, in *IEEE 1992 Ultrason. Symp. Proc.*, vol. 1, pp. 603–607 (IEEE Cat. No. 92CH3118-7).

[13] Lu, J-y., and Greenleaf, J. F., A computational and experimental study of nondiffracting transducer for medical ultrasound, *Ultrasonic Imaging 12*, 146–147 (1990) (abstract).

[14] Lu, J-y., and Greenleaf, J. F., Effect on J_0 Nondiffracting beam of deleting central elements of J_0 annular array transducer, *Ultrasonic Imaging 13*, p. 203 (1991) (abstract).

[15] Lu, J-y., and Greenleaf, J. F., Simulation of imaging contrast of nondiffracting beam transducers, *J. Ultrasound Med. 10*, p. S4 (1991) (abstract).

[16] Lu, J-y., and Greenleaf, J. F., Experiment of imaging contrast of J_0 Bessel nondiffracting beam transducer, *J. Ultrasound Med. 11*, p. S43 (1992) (abstract).

[17] Lu, J-y., and Greenleaf, J. F. Sidelobe reduction of nondiffracting pulse-echo images by deconvolution, *Ultrasonic Imaging 14*, p. 203 (1992) (abstract).

[18] Lu, J-y., and Greenleaf, J. F., New development in beam propagation, *J. Ultrasound Med. 12*, p. S29 (1993) (abstract).

[19] Campbell, J. A., and Soloway, S., Generation of a nondiffracting beam with frequency independent beam width, *J. Acoust. Soc. Am. 88*, 2467–2477 (1990).

[20] Lu, J-y., and Greenleaf, J. F., Nondiffracting X waves — exact solutions to free-space scalar wave equation and their finite aperture realizations, *IEEE Trans. Ultrason. Ferro. Freq. Control 39*, 19–31 (1992).

[21] Lu, J-y., and Greenleaf, J. F., Experimental verification of nondiffracting X waves, *IEEE Trans. Ultrason. Ferro. Freq. Control 39*, 441–446 (1992).

[22] Lu, J-y., and Greenleaf, J. F., Theory and Acoustic Experiments of Nondiffracting X Waves, in *IEEE 1991 Ultrason. Symp. Proc.*, vol. 2, pp. 1155–1159 (IEEE Cat. No. 91CH3079-1).

[23] Fatemi, M., and Arad, M. A., A Novel Imaging System Based on Nondiffracting X Waves, in *IEEE 1992 Ultrason. Symp. Proc.* vol. 1, pp. 609–612 (IEEE Cat. No. 92CH3118-7).

[24] Foster, F. S., Larson, J. D., Pittaro, R. J., Corl, P. D., Greenstein, A. P. and Lum, P. K., A digital annular array prototype scanner for real-time ultrasound imaging, *Ultrasound Med. Biol. 15*, 661–672 (1989).

[25] John, F., *Partial Differential Equations* (Springer-Verlag, New York, 1982).

[26] Rosenfeld, A., and Kak, A. C., *Digital Picture Processing* (Academic Press, New York, 1982).

[27] Fatemi, M., and Arad, M. A., Ultrasonic Nondiffracting Beam Image Formation and Restoration, in *IEEE 1991 Ultrason. Symp. Proc.*, vol. 2, pp. 1305–1308 (IEEE Cat. No. 91CH3079-1).